

Astronomical Journal, 2007, (October), in press

HST Observations of Chromospheres in Metal Deficient Field Giants

A. K. Dupree, and Timothy Q. Li

*Harvard-Smithsonian Center for Astrophysics,
Cambridge MA 02138*

adupree@cfa.harvard.edu

and

Graeme H. Smith

UCO/Lick Observatory, University of California, Santa Cruz, CA 95064

graeme@ucolick.edu

ABSTRACT

HST high resolution spectra of metal-deficient field giants more than double the stars in previous studies, span ~ 3 magnitudes on the red giant branch, and sample an abundance range $[\text{Fe}/\text{H}] = -1$ to -3 . These stars, in spite of their age and low metallicity, possess chromospheric fluxes of Mg II ($\lambda 2800$) that are within a factor of 4 of Population I stars, and give signs of a dependence on the metal abundance at the lowest metallicities. The Mg II k-line widths depend on luminosity and correlate with metallicity. Line profile asymmetries reveal outflows that occur at lower luminosities ($M_V = -0.8$) than detected in Ca K and H-alpha lines in metal-poor giants, suggesting mass outflow occurs over a larger span of the red giant branch than previously thought, and confirming that the Mg II lines are good wind diagnostics. These results do not support a magnetically dominated chromosphere, but appear more consistent with some sort of hydrodynamic, or acoustic heating of the outer atmospheres.

Subject headings: stars:chromospheres; stars: winds, outflows; stars: Population II; ultraviolet: stars

1. Introduction

Red giant stars of the Galactic halo have extremes in a number of properties, such as age, metal abundances, and space motion, that have made them useful probes of the early evolution of the Galaxy. It is well established that the chromospheric activity of stars decreases with increasing age on the main sequence (e.g., Soderblom 1985; Soderblom et al. 1991, Dravins et al. 1993) In addition, observations show that the fluxes in chromospheric and transition region emission lines decrease as stars evolve into the red giant phase (e.g., Schrijver 1987; Simon & Drake 1989; Böhm-Vitense 1992). Consequently, red giants of the Galactic halo present us with the opportunity to study the extreme limits of another phenomenon, namely stellar activity.

Due to the faintness of even the closest Population II red giants, investigation of their chromospheres has so far centered around three spectroscopic features: emission in the wings of the $H\alpha$ line, in the cores of the Ca II H and K lines, and in the cores of the Mg II h and k lines. Metal-poor giants brighter than $\log(L/L_\odot) \sim 2.5$ (Cacciari et al. 2004) in both the halo field and globular clusters frequently exhibit emission in one or both of the wings of the $H\alpha$ absorption line (e.g., Cohen 1976; Mallia & Pagel 1978; Cacciari & Freeman 1983, Gratton et al. 1984; Smith & Dupree 1988; Bates et al. 1993; Kemp & Bates 1995). Lyons et al. (1996) conclude that $\approx 80\%$ of a total of 68 stars from five globular clusters with $\log(L/L_\odot) > 2.7$ exhibit $H\alpha$ emission. The emission profiles are more often than not asymmetric with one wing being stronger than the other. However the strengths of the emission change with time.

Next to the $H\alpha$ emission features, the most extensively studied chromospheric diagnostics among Population II giants are the central emission reversals in Ca II H and K lines. Spectroscopic studies of these emission components in both halo field and globular cluster red giants have been reported by Dupree et al. (1990a), Smith et al. (1992), Dupree & Smith (1995), and Cacciari et al. (2004). The presence of Ca II H and K emission is detected further down the red giant branch of Population II stars than is emission in the wings of $H\alpha$. The profiles of the Ca emission cores of metal-poor giants are often asymmetric, with the sense of the asymmetry changing from blue-dominant to red-dominant with increasing luminosity on the giant branch. Chromospheric emission in the H and K lines has also been documented among metal-poor subdwarfs (Smith & Churchill 1998), and in the case of at least one such star, HD 103095, which was included in the Mount Wilson HK survey, an activity cycle of period 7.3 yr has been detected (Baliunas et al. 1995).

The asymmetries and time variability of the $H\alpha$ and Ca II emission profiles are consistent with the presence of outflows within the chromospheres of metal-poor stars on the upper giant branch (e.g., Dupree et al. 1984; Mauas et al. 2006). This evidence is supported by the onset of blueshifts in the $H\alpha$ at luminosities slightly lower than the onset of $H\alpha$ emission,

and blueshifts in NaD line cores at higher luminosities (e.g., Peterson 1981; Shetrone 1994; Kemp & Bates 1995; Shetrone & Keane 2000; Cacciari et al. 2004). Furthermore, wind signatures have been found in the $\lambda 10830$ He I line of a small number of Population II field giants (Dupree et al. 1992; Smith et al. 2004).

The Mg II chromospheric emission lines, analyzed for cool stars of approximately solar abundance by Cardini (2005), have been less studied among metal-poor giants where metallicity effects can be addressed. Work based on *IUE* observations of field giants has been presented by Dupree et al. (1990b), while a *HST* GHRS spectrum of HD 216143 was discussed by Smith & Dupree (1998). The Mg II emission in red giants of the globular cluster NGC 6752 have been studied using both *IUE* and *HST* GHRS (Dupree et al. 1990a, 1994). Despite having metallicities of a factor of 100 or more less than solar, the Mg II emission fluxes among the Dupree et al. (1990b) sample were in some cases not substantially less than those of Population I giants and supergiants. Cuntz et al. (1994) found that this relative insensitivity of emission flux to metallicity can be accounted for by an acoustic-heating model for red giant chromospheres.

High-resolution Mg II *HST* spectra of nine metal-poor subdwarf stars with $-2.2 < [\text{Fe}/\text{H}] < -0.6$ were obtained by Peterson & Schrijver (1997). They found that at $[\text{Fe}/\text{H}] < -1.0$ the emission fluxes were no more than a factor of three less than that of the solar-like dwarf α Cen A. Their observations suggest that the subdwarf progenitors of metal-poor halo red giants have significant levels of chromospheric activity, perhaps even comparable to quiet regions on the Sun. They suggested that these subdwarfs also have acoustically-heated chromospheres.

The available evidence shows therefore that metal-poor halo stars, despite being of great age, do nonetheless have chromospheres with levels of activity perhaps not very dissimilar from that of the quiet Sun. The strongest of this evidence comes from the fluxes of the Mg II *h* and *k* emission lines, which have profiles that show more contrast with the photospheric spectrum than either the Ca II H-K or H α lines. Given that much of the Mg II spectroscopy of metal-poor red giants came from the *IUE* spacecraft, this is an area in which *HST* archival data can contribute substantially.

2. Data

High resolution spectra of the $\lambda 2800$ Mg II lines in metal-poor red giants were taken from the *HST* archives for the metal-poor red giants listed in Table 1. The position of the stars on a color-magnitude diagram is shown in Fig. 1, where the dataset spans more than 3

magnitudes for stars on the red giant branch and asymptotic giant branch, and abundances are less than solar by factors of 10 to 1000. The spectra for all but three of these stars were obtained during *HST* Cycle 8 as part of a study of the abundances of *r*-process heavy elements in metal-poor red giants (Proposal 8342, PI J. Cowan). The E230M echelle grating was used with *HST*-STIS to obtain spectra covering the wavelength range $\lambda\lambda 2410\text{-}3070$ with a resolution of 0.09 \AA at the $\lambda 2800$ Mg II lines. The STIS spectrum of HD 122563 was obtained with a similar setup as part of Program 8111 (PI C. Sneden). Abundance analyses based on these spectra are discussed by Cowan et al. (2005). By contrast, GHRS spectra of HD 6833 and HD 216143 were obtained from the datasets of Proposals 6010 and 6511 (PIs J. Bookbinder and G. Smith respectively). The Mg II spectrum of HD 216143 from these data has been previously discussed by Smith & Dupree (1998). Specific details of the individual spectra are given in Table 2.

Spectroscopic metallicities are available in the literature for all of the stars in Table 1. The $[\text{Fe}/\text{H}]$ metallicities listed in column 9 come from three different sources referred to in column 10, namely Fulbright (2000), Johnson (2002), and McWilliam et al. (1995b), all of whom employed high-resolution spectra. In the case of the latter two of these references the quoted value of $[\text{Fe}/\text{H}]$ is based on analysis of Fe I lines. To give a sense of the uncertainties in these metallicities, the values of $[\text{Fe}/\text{H}]$ from Cowan et al. (2005) are listed in column 11 for comparison with the other literature values.

The spectra are shown in a stacked presentation in Figures 2 and 3, aligned according to a photospheric wavelength scale. The zero-point for each spectrum (marked by broken lines) is offset from that of the spectrum below it by an amount equal to $2 \times 10^{-13} \text{ erg cm}^{-2} \text{ s}^{-1}$. In addition, some of the spectra with the lowest flux levels have been further scaled by an arbitrary factor. The expected positions of the interstellar Mg II *h* and *k* absorption features are shown by vertical lines. In many cases these are shifted well away from the stellar chromospheric emission profiles as a result of large stellar radial velocities. Thus, the typical central reversal of chromospheric emission line profiles becomes apparent in these objects. However, for some stars (many of the stars in Figure 2 and HD 115444 in Figure 3), the ISM absorption is superimposed on the chromospheric lines, and in giants such as HD 122563 and HD 165195 significantly alters the apparent line asymmetry and affects the observed line fluxes.

In most cases the stars exhibit asymmetric *h* and *k* profiles with the sense of the asymmetry being consistent between the two lines. Two notable exceptions are HD 122956 and HD 6833. In the former case the profiles are nearly symmetric and the degree of asymmetry is mild. In the case of HD 6833 the *k* line is pronouncedly asymmetric ($V/R < 1$) while the *h* line shows a modest asymmetry in the opposite sense. By contrast, *IUE* spectra obtained

in 1984 showed similar h and k profiles (see Figure 2 of Dupree et al. 1990b). Evidently the asymmetry of this star is time variable. In the case of the star α Ori a self-absorbed Mn I resonance line absorbs the short wavelength emission of the Mg II k line (see Figure 5 of Lobel & Dupree 2000) leading to an apparent asymmetry. However, this effect is not likely to be the cause of the red asymmetry in the *HST* spectrum of the HD 6833 k line because this line is narrower than for α Ori so that the Mn I line lies outside the emission core. The k line is formed at higher atmospheric levels than the h line which could support different velocity fields in a dynamic atmosphere.

3. Emission Line Fluxes

The chromospheric fluxes in the Mg II emission cores were measured from the spectra by summing directly over the emission profiles between the flux minima on either side without correcting for any photospheric contribution to the line. While this procedure is straightforward, it will overestimate the amount of chromospheric emission by including some photospheric contribution near the line profile minima. The photospheric Mg II lines are extremely deep, however, practically reaching the zero level near line center, and as such are expected to contribute a relatively small amount to the derived fluxes.

To investigate this point, R. Kurucz kindly computed synthetic spectra for two of the hottest stars in our sample, HD 6755 and HD 175305, for which the greatest photospheric fluxes would be expected within the wavelength ranges encompassed by the emission cores. Pure radiative models were constructed using the latest version of Kurucz (2005) model atmospheres. Such models contain an isothermal atmosphere in hydrostatic equilibrium extended until the density falls to negligible values. The assumption is that no additional heating is present to produce a rise in atmospheric temperature. A chromosphere is absent and the synthesized spectrum represents only the photospheric contribution. The Mg and Ca abundances for these models were enhanced by 0.3 dex over the Fe values based on the fine analysis by Fulbright (2000). The atmospheric parameters (Carney et al. 2003) adopted for these models were $T_{\text{eff}} = 5080\text{K}$, $[\text{Fe}/\text{H}] = -1.7$, $\log g = 2.7$ (corresponding to $M_V = 1.5$), and $v_{\text{tot}} \sin i = 3.5 \text{ km s}^{-1}$ for HD 6755, with $T_{\text{eff}} = 5050 \text{ K}$, $[\text{Fe}/\text{H}] = -1.4$, $\log g = 2.8$ ($M_V = 1.8$), and $v_{\text{rot}} \sin i = 1.5 \text{ km s}^{-1}$ for HD 175305. Although we have adopted a small rotational velocity for HD 6755 this star is a spectroscopic binary (Carney et al. 2003). However, with a period of 1641 days it shouldn't be rotating very fast, although there is the uncertainty of whether the spectrum contains some light from the companion.

The Kurucz photospheric models are overplotted on the observed Mg II spectra in Figures 4 and 5. In both cases, over the wavelength range bounded by the flux minima on either

side of the emission profile, the net flux in the photospheric Mg II lines is relatively small by comparison with the integrated chromospheric emission. Subtracting the contribution of the synthesized photospheric flux model to the integrated Mg II emission amounts to a correction of less than 12 percent. For the remainder of the stars, we fit a local continuum, in the form of a second-order polynomial, to the minima on each side of the emission (the k_1 and h_1 locations). The difference between the total flux measured from zero and the continuum-removed flux can amount to 30%. One star, HD 122563, is an exception where it is a factor of 2.1 smaller due to the high continuum level (see Figure 2), and this continuum subtracted flux is used here (Table 3). However, this star, and four others have radial velocities comparable to that of the local interstellar medium. As a result, the observed emission is reduced by interstellar Mg II absorption. A previous study (Dupree et al. 1990b) of the effects of interstellar absorption on high latitude metal deficient stars with low reddening, concluded that the stellar flux could be increased by $\sim 25\%$ if interstellar absorption were absent. We have marked these stars in Table 3, and the fluxes are displayed in the figures as lower limits.

The k and h emission fluxes measured from the *HST* spectra are listed in columns 2 and 3 of Table 3. The total observed flux F_{obs} for the two lines combined is listed in column 4. These fluxes at Earth were converted to fluxes at the surface of each star through use of the Barnes et al. (1978) relation to calculate the stellar angular diameter ϕ (in units of 10^{-3} arcsec) from the stellar $(V - R)_0$ color. These diameters are listed in column 5 of Table 3. A stellar surface flux in units of $\text{erg cm}^{-2} \text{s}^{-1}$ was then calculated from the relation

$$F_{\text{Mg II}} = F_{obs}(d/R_\star)^2 = F_{obs} \times 1.702 \times 10^{17}/\phi^2, \quad (1)$$

where R_\star is the stellar radius, and corrected for reddening according to the $E(B - V)$ values from Table 1 and $A_{\lambda 2800} = 6.1E(B - V)$ (Seaton 1979; Cardelli et al. 1989). The values of $F_{\text{Mg II}}$ are listed in column 6 of Table 3, while column 7 gives their ratio to the solar Mg II emission flux.

The Mg II fluxes of the metal-poor giants are much less than that of the Sun as a star, but the relevant comparison for our purposes is to other red giant stars of higher metallicity. The observed Mg II surface fluxes measured from the *HST* spectra are plotted versus $(V - R)_0$ in Figure 6. This figure also includes data from Dupree et al. (1990b) for metal-poor field giants observed with *IUE* (Table 4), updated using values of $E(B - V)$ and $[\text{Fe}/\text{H}]$ from Pilachowski et al. (1996), McWilliam et al. (1995a,b), Fulbright et al. (2000), Beers et al. (2000), and Burris et al. (2000). In addition, the fluxes compiled by Dupree et al. for Population I supergiants, Hyades giants, and M67 giant stars (Tables 5, 6 and 7) are also shown. Dupree et al. (1990b) found that the surface fluxes of metal-poor giants in their smaller sample were comparable to those of near-solar abundance giants. A similar effect

can be seen in Figure 6 with most of the metal-poor giants falling close to the Population I sequence except for stars near $(V - R)_0 \sim 0.8$. Four metal-poor stars in this region have lower limits on their surface fluxes. While the correction for interstellar Mg II absorption will increase the stellar flux, it does not appear likely that the flux will increase by 0.5 dex, or a factor of 3 or more to bring them up to the Population I stars. Interestingly, the M67 giants, which are about 0.2 mag redder in $(V - R)_0$ show a similar trend.

Despite the similarity between the Mg II surface fluxes of metal-poor and Population I giants, these fluxes do show a correlation with $[\text{Fe}/\text{H}]$ as shown in Figure 7. In fact they appear to show less scatter in this figure at a given $[\text{Fe}/\text{H}]$ than in Figure 6 at a fixed $(V - R)_0$, suggesting that the trend seen with $[\text{Fe}/\text{H}]$ may be more than an artifact of the relation between red giant color and metallicity.¹ Based upon this evidence, the giants which fall below the mean sequence in Figure 6 do so as a result of this metallicity effect. The most discrepant metal-poor stars in Figure 6 with $(V - R)_0 < 0.87$ and Mg II surface fluxes less than $10^5 \text{ erg cm}^{-2} \text{ s}^{-1}$ are HD 6268, 115444, 122563, 126587, and 186478. They all have metallicities of $[\text{Fe}/\text{H}] < -2.5$. Some of the scatter in Figures 6 and 7 might be due to variability. High quality *IUE* spectra of cool stars have shown a difference up to a factor of 2 in fluxes of the Mg II lines, measured at different times when the expected error of measurement is $\leq \pm 20\%$ (Brocius et al. 1985; Dupree et al. 1987).

4. Line Profiles

4.1. Asymmetries

The asymmetries of the Mg II *k*-line profiles from the *HST* spectra are shown in Figure 8 as a function of position in the color-magnitude diagram using the values in Table 1. Stars are plotted with symbols designating the *V/R* parameter, which refers to the ratio between the maximum intensities in the violet (short-wavelength) and red (long-wavelength) peaks of the *k*-line emission profile. The 8 stars are plotted whose radial velocities place them away from the local interstellar Mg II absorption, the presence of which could affect the asymmetry. The most luminous stars show outflow signatures, in that the violet emission is less than the red emission. The long broken line at $M_V = -1.7$ marks the lower extent of the region where asymmetries of $V/R < 1$ and K_3 absorption reversal blue-shifts dominate in the Ca II K_2 emission-line profile as determined from the metal-poor field giant spectroscopy

¹In fact, a color-metallicity relation coupled with the trend seen in Figure 6, would cause a more metal-poor (bluer) star to have a higher surface flux than a metal-richer giant, the opposite of what is seen in Figure 7.

of Smith et al. (1992) and Dupree & Smith (1995). In the globular cluster NGC 2808, which has a metallicity of $[\text{Fe}/\text{H}] = -1.14$ (Carretta et al. 2004), Cacciari et al. (2004) find a similar limit to the $V/R < 1$ asymmetry of the Ca II K-line. The Mg II emission is formed higher in the extended stellar atmosphere, and is consequently more sensitive to accelerating outflows than the emission lines formed in the lower chromosphere. Population I giants show the same signature in Mg II at similar luminosities (Stencel & Mullan 1980; Böhm-Vitense 1981) indicated by the short-dashed line in Figure 8. Anthony-Twarog & Twarog (1994) evaluated the reddening and derived absolute magnitudes for these stars from *uvby* photometry, and their values are used in Figure 9. The position of our target stars with respect to the Population I objects remains similar to that in Figure 8.

4.2. Wilson-Bappu Emission Line Widths

Widths of the Mg II k lines were measured following the precepts of Cassatella et al. (2001). The observed width is taken to be the full width of a fitted Gaussian profile (deleting the central absorption reversal from the fit), measured at the half maximum value of the observed line peak. Correction was made for the instrumental broadening by assuming that the measured width is a quadratic sum of the intrinsic stellar width W_0 and a resolution element. We omitted three stars where the emission was very weak and the spectrum noisy (HD 115444) or the interstellar absorption seriously compromised the wing of the line (HD 6268 and HD 186478). The line widths are plotted as a function of M_V in Figure 10 using the Bond (1980) data, and in Figure 11 for absolute magnitudes from Anthony-Twarog & Twarog (1994). This is the Mg II equivalent of the Wilson-Bappu (1957) relation for metal-poor giants. Also shown in these figures as a broken line is the mean Wilson-Bappu relation for Population I giants as derived by Cassatella et al. (2001) for a large sample of stars for which high-resolution *IUE* spectra and *Hipparcos* parallaxes are available. The Cassatella et al. relation (their equation 3) is

$$M_V = (34.56 \pm 0.29) - (16.75 \pm 0.14) \log(W_0 \text{ km s}^{-1}). \quad (2)$$

The dispersions in line width at a given M_V among the Cassatella et al. (2001) sample are shown by the shaded regions in Figures 10 and 11, which depict the 50–67% extent in the values of $\log W_0$ among stars within bins of one-magnitude width. The metal-poor red giants have k emission profiles that are narrower than the bulk of the Cassatella et al. sample (and in some cases, narrower than all the stars) and certainly more narrow than the mean relation for the sample.

A similar situation was found for the Ca II K₂ lines of metal-poor red giants by Dupree & Smith (1995). By contrast, from their spectroscopy of red giants in NGC 2808, Cacciari

et al. (2004) found no evidence for a metallicity dependence of the Wilson-Bappu effect in Ca II K₂. The stars in this *HST* sample all have metallicities much lower than NGC 2808 ([Fe/H]=−1.14, Carretta et al. 2004), so that our sample would be more likely to reveal a metallicity dependence to the Wilson-Bappu effect. The difference between the observed line width $\log W_0$ and that given by equation (2) is plotted against [Fe/H] in Figure 12 for the metal-poor giants in the *HST* sample. This figure does reveal evidence of a correlation, with the deviation from the Cassatella et al. relation being greater for lower metallicities. These figures therefore provide evidence for a metallicity dependence to the Wilson-Bappu effect for the Mg II *k* line. Since the line widths of the metal-poor giants are consistently less than predicted by the Cassatella et al. (2001) relation for their absolute magnitude, values of M_V would be underestimated if based on the observed Mg II *k* width.

5. Discussion

Results from the *HST* spectra reported in this paper extend and confirm those found previously (Dupree et al. 1990b) in showing that the Mg II chromospheric emission fluxes of metal-poor Population II red giants are comparable to or within a factor of ~ 4 of Population I giants and supergiants of similar $(V - R)_0$ color. This behavior, in spite of [Fe/H] ratios that are factors of 10 to 1000 less than the Population I stars and that our sample is older, suggests a different chromospheric structure and heating mechanisms from Population I stars must be present in these halo red giants. The *HST* data do provide the first evidence that the Mg II emission fluxes correlate with [Fe/H], at least for [Fe/H] < −2.0 (Figure 7). At higher metallicities this trend may flatten out although the number of stars in our sample is really too small to be definitive on this point. This metallicity effect may provide an explanation for the range in $\log F_{\text{Mg II}}$ seen among stars with $(V - R)_0 \sim 0.7$ to 1.0 in Figure 6. One limitation of the present *HST* sample is that the color range is fairly restricted, so we cannot conclude very much about metal-poor giants outside this range, except that the four such stars in Figure 6 do superimpose on the Population I sequence.

Although the most metal-poor stars in our sample have [Mg/H] < −2 (such stars have [Mg/Fe] ≤ 0.4 ; Hanson et al. 1998), they have Mg II emission fluxes no less than about 0.6–0.7 dex that of Population I giants and supergiants. Peterson & Schrijver (1997) reported similarly that for subdwarfs the Mg II emission flux did not scale strongly with metallicity. They suggested that subdwarfs may have chromospheres similar to that of the quietest regions of the Sun. The picture that emerges for metal-poor Population II stars is that their chromospheres may evolve analogously to those of quiet Population I stars. The similarity in $F_{\text{Mg II}}$ between the M67 and the least active metal-poor giants in Figure 6 may be consistent

with this suggestion.

The metal-poor giants in Figure 6 are both older and much more metal-deficient than the evolved Population I stars to which they are compared. Magnetic processes, direct or indirect, play a role in chromospheric heating of a star like the Sun (Judge et al. 2003), but the contribution of heating through dissipation of acoustic waves remains controversial (Cuntz et al. 2007; Fossom & Carlsson 2006; Wedemeyer-Böhm et al. 2007). Since the stellar dynamo within a main sequence star does decline with time it may be that in Population II stars the trends in chromospheric Mg II emission are being driven largely by an acoustic heating of the chromosphere, as argued by Peterson & Schrijver (1997). Variable profile asymmetries of H α in metal deficient giants led Smith & Dupree (1988) to identify pulsation as a likely source of heating and momentum deposition. A consideration here could involve the energy balance. If the energy input were similar in both metal-rich and metal-poor atmospheres, the fact that radiative cooling is decreased in the metal-poor chromospheres could lead to a warmer atmosphere and increase the Mg II emission, thus compensating for the decreased Mg abundance.

Cuntz et al. (1994) have explained the insensitivity of the Mg II emission-line fluxes of cool giant stars to metallicity in terms of acoustic shock-wave heated chromospheric models. These models account for a basal, i.e., non-magnetic, component (e.g., Schrijver 1987; Rutten et al. 1991) in the fluxes of the Mg II and Ca II emission lines of late-type stars (Buchholz et al. 1998). Cuntz et al. computed the run of physical conditions with height within red giant chromospheres of various metallicity into which the same acoustic flux is input in the form of propagating shock waves. As the metallicity of the chromosphere is reduced the bulk of the Mg II k line emission tends to be formed deeper at higher mass column densities. Cuntz et al. (1994) computed the physical height in their models at which the optical depth across the k line profile (computed in plane-parallel geometry) was equal to unity for metallicities ranging from Z_{\odot} to $Z_{\odot}/100$. Across this resulting range in heights the temperature and velocity structure of their shock models did not vary greatly with either metallicity or altitude. Thus even though the physical line formation depth does vary with metallicity, the line was always formed under conditions of similar temperature and velocity structure. As a result, the emission flux was found not to vary greatly with metallicity.

Despite the success of these acoustic models, magnetic heating may still play a role in maintaining the chromospheres of Population II stars, at least during some phases of their evolution. The evidence of the subdwarf HD 103095 ($[\text{Fe}/\text{H}] = -1.2$, Balachandran & Carney 1996) suggests that magnetic activity cycles may be present on the main sequence (Baliunas et al. 1995), although with a color of $B - V = 0.75$ this star is much cooler than the main sequence progenitors of the red giants in Table 1. Main sequence turnoff stars

with a metallicity of $[\text{Fe}/\text{H}] = -2.3$, $[\alpha/\text{Fe}] = 0.3$, and ages of 12–14 Gyr have colors of $(B - V)_0 \sim 0.325\text{--}0.35$ and effective temperatures of $\log T_{\text{eff}}(\text{K}) \sim 3.83$ to 3.82 (see Figures 11 and 12 of Bergbusch & Vandenberg 2001), i.e., $T_{\text{eff}} = 6760\text{--}6610$ K. These are similar in temperature to low-mass Population I F2-F5 V stars (Bessell 1979). Simon & Landsman (1991) found that C II 1335 Å emission among Population I F dwarfs earlier than spectral type F5 is uncorrelated with rotation, supporting the idea that the chromospheres of A and early-F dwarfs are heated by the shock dissipation of acoustic waves. Thus the main sequence progenitors of the metal-poor giants in Table 1 are expected to have had acoustically-heated chromospheres. When they evolve off the main sequence towards cooler effective temperatures such stars may transition to chromospheres that have a dynamo contribution to the heating, as suggested by Simon & Drake (1989) for Population I giants. Clump giants in the Hyades clearly give evidence for magnetic activity (Baliunas et al. 1983). By the time that they evolve beyond the luminosity of the horizontal branch, however, it may be that old metal-poor giants have returned to chromospheres that are mainly heated by acoustic processes.

Among Population I giants evidence exists for both acoustic and magnetic heating of the chromosphere. Observations of Population I G and K giants in similar evolutionary states do show evidence for correlations between chromospheric emission line fluxes, X-ray fluxes, and rotation (Strassmeier et al. 1994; Gondoin 2005). The evolution of X-ray emission with advancing evolution away from the main sequence depends on stellar mass; for low-mass stars ($M < 1.5 M_{\odot}$) the X-ray activity decreases with evolution away from the main sequence, while for intermediate-mass giants ($1.5 M_{\odot} < M < 3.0 M_{\odot}$) the activity at first increases up to a spectral type of around K1, beyond which it drops (Pizzolato et al. 2000; Gondoin 1999, 2005). During the red giant phase of evolution of Population I stars up to colors as red as $B - V \sim 1.2$, a dynamo may contribute to chromospheric activity, but with advanced evolution to the higher luminosities and cooler temperatures of the later K giants the radiative energy losses in the Mg II and other emission lines can approach the “basal” levels observed among red giants by Schrijver (1987) and Judge & Stencel (1991), which they attribute to acoustic shock heating. The evolution of Ca II H and K emission fluxes among the red giants of the solar-age open cluster M67 seems consistent with this scenario (Dupree et al. 1999). The chromospheric evolution of Population II giants may be analogous to those of Population I, with the modification that the greater ages of the progenitors of the former stars has reduced the magnetic-heating contribution, so that the acoustic component is relatively more important.

It will be important to use the next generation of HST instruments to probe the onset of outflows to fainter magnitudes and access a more homogeneous sample of stars represented by globular cluster members.

We are grateful to Chris Sneden who called our attention to these spectra from his program and made them available for analysis. The SIMBAD reference catalogue produced by the Centre de Données astronomiques de Strasbourg was extremely useful. The MAST Archive at STScI provided the HST spectra. This work was supported in part by NASA.

Facility: HST (GHRS, STIS), IUE

REFERENCES

- Anthony-Twarog, B. J., & Twarog, B. A. 1994, *AJ*, 107, 1577 [AT94]
- Balachandran, S. C., & Carney, B. W. 1996, *AJ*, 111, 946
- Baliunas, S. L., Hartmann, L., & Dupree, A. K. 1983, *ApJ*, 271, 672
- Baliunas, S. L., et al. 1995, *ApJ*, 438, 269
- Barnes, T. G., Evans, D. S., & Moffett, T. J. 1978, *MNRAS*, 183, 285
- Bates, B., Kemp, S. N., & Montgomery, A. S. 1993, *A&A*, 97, 937
- Beers, T. C., Chiba, M., Yoshii, Y., Platais, I., Hanson, R. B., Fuchs, B., & Rossi, S. 2000, *AJ*, 119, 2866
- Bergbusch, P. A., & Vandenberg, D. A. 2001, *ApJ*, 556, 322
- Bessell, M. S. 1979, *PASP*, 91, 589
- Böhm-Vitense, E. 1981, *ApJ*, 244, 504
- Böhm-Vitense, E. 1992, *AJ*, 103, 608
- Bond, H. E. 1980, *ApJS*, 44, 517 [B80]
- Brosius, J. W., Mullan, D. J., & Stencel, R. E. 1985, *ApJ*, 288, 310
- Buchholz, B., Ulmschneider, P., & Cuntz, M. 1998, *ApJ*, 494, 700
- Burris, D. L., Pilachowski, C. A., Armandroff, T. E., Sneden, C., Cowan, J. J., & Roe, H. 2000, *ApJ*, 544, 302
- Cacciari, C., & Freeman, K. C. 1983, *ApJ*, 268, 185

- Cacciari, C., Bragaglia, A., Rossetti, E., Fusi Pecci, F., Mulas, G., Carretta, E., Gratton, R. G., Momany, Y., & Pasquini, L. 2004, *A&A*, 413, 343
- Cardelli, J. A., Clayton, G. C., & Mathis, J. S. 1989, *ApJ*, 345, 245
- Cardini, D. 2005, *A&A*, 430, 303
- Carney, B. W. 1980, *AJ*, 85, 38
- Carney, B. W., Latham, D. W., Stefanik, R. P., Laird, J. B., & Morse, J. A. 2003, *AJ*, 125, 293
- Carretta, E., Bragaglia, A., & Cacciari, C. 2004, *ApJ*, 610, L25
- Cassatella, A., Altamore, A., Badiali, M., & Cardini, D. 2001, *A&A*, 374, 1085
- Cohen, J. G. 1976, *ApJ*, 203, L127
- Cousins, A. W. J. 1976, *Mem. R. A. S.*, 81, 25
- Cowan, J. J., Sneden, C., Beers, T. C., Lawler, J. E., Simmerer, J., Truran, J. W., Primas, F., Collier, J., & Burles, S. 2005, *ApJ*, 627, 238
- Cuntz, M., Rammacher, W., & Ulmschneider, P. 1994, *ApJ*, 432, 690
- Cuntz, M., Rammacher, W., & Musielak, Z. E. 2007, *ApJ*, 657, L57
- Dravins, D., Linde, P., Ayres, T. R., Linsky, J. L., Monsignori-Fossi, B., Simon, T., & Wallinder, F. 1993, *ApJ*, 403, 412
- Dupree, A. K., & Smith, G. H. 1995, *AJ*, 110, 405
- Dupree, A. K., Hartmann, L., & Avrett, E. H. 1984, *ApJ*, 281, L37
- Dupree, A. K., Baliunas, S. L., Guinan, E. F., Hartmann, L., Nassiopoulos, G. E., & Sonneborn, G. 1987, *ApJ*, 317, L85
- Dupree, A. K., Harper, G. M., Hartmann, L., Jordan, C., Rodgers, A. W., & Smith, G. H. 1990a, *ApJ*, 361, L9
- Dupree, A. K., Hartmann, L., & Smith, G. H. 1990b, *ApJ*, 353, 623
- Dupree, A. K., Sasselov, D. D., & Lester, J. B. 1992, *ApJ*, 387, L85
- Dupree, A. K., Hartmann, L., Smith, G. H., Rodgers, A. W., Roberts, W. H., & Zucker, D. B. 1994, *ApJ*, 421, 542

- Dupree, A. K., Whitney, B. A., & Pasquini, L. 1999, *ApJ*, 520, 751
- Fossum, A., & Carlsson, M. 2006, *ApJ*, 646, 579
- Fulbright, J. P., 2000, *AJ*, 120, 1841
- Gondoin, P. 1999, *A&A*, 352, 217
- Gondoin, P. 2005, *A&A*, 444, 531
- Gonzalez, G., & Wallerstein, G. 1998, *AJ*, 116, 765
- Gratton, R. G., Pilachowski, C. A., & Sneden, C. 1984, *A&A*, 132, 11
- Hanson, R. B., Sneden, C., Kraft, R. P., & Fulbright, J. 1998, *AJ*, 116, 1286
- Hartmann, L., Dupree, A. K., & Raymond, J. C. 1982, *ApJ*, 252, 214
- Hartmann, L., Jordan, C., Brown, A., & Dupree, A. K. 1985, *ApJ*, 296, 576
- Janes, K. A., & Heasley, J. N. 1988, *AJ*, 95, 762
- Janes, K. A., & Smith, G. H. 1984, *AJ*, 89, 487
- Johnson, H. L., & Sandage, A. R. 1955, *ApJ*, 121, 616
- Johnson, H. L., Iriarte, B., Mitchell, R. I., & Wisniewskj, W. Z. 1966, *Comm. Lunar Planet. Lab.*, 4, 99
- Johnson, J. A. 2002, *ApJS*, 139, 219
- Judge, P. G., & Stencel, R. E. 1991, *ApJ*, 371, 357
- Judge, P. G., Carlsson, M., & Stein, R. F. 1983, *ApJ*, 597, 1158
- Kemp, S. N., & Bates, B. 1995, *A&AS*, 112, 513
- Kurucz, R. L. 2005, *Mem. Soc. Astron. Ital. Supp.*, 8, 14
- Lobel, A., & Dupree, A. K. 2000, *ApJ*, 545, 454
- Lyons, M. A., Kemp, S. N., Bates, B., & Shaw, C. R. 1996, *MNRAS*, 280, 835
- Mallia, E. A., & Pagel, B. E. J. 1978, *MNRAS*, 184, P55
- Mauas, P. J. D., Cacciari, C., & Pasquini, L. 2006, *A&A*, 454, 609

- McWilliam, A., Preston, G. W., Sneden, C., & Shectman, S. 1995a, *AJ*, 109, 2736
- McWilliam, A., Preston, G. W., Sneden, C., & Searle, L. 1995b, *AJ*, 109, 2757
- Murray, C. A., & Clements, E. D. 1968, *Royal Obs. Bull.*, No. 139, 309
- Peterson, R. C. 1981, *ApJ*, 248, L31
- Peterson, R. C., & Schrijver, C. J. 1997, *ApJ*, 480, L47
- Pilachowski, C., Sneden, C., & Kraft, R., 1996, *AJ*, 111, 1689
- Pizzolato, N., Maggio, A., & Sciortino, S. 2000, *A&A*, 361, 614
- Ridgway, S. J. Joyce, R. R., White, N. M., & Wing, R. F. 1980, *ApJ*, 235,126
- Rutten, R. G. M., Schrijver, C. J., Lemmens, A. F. P., & Zwaan, C. 1991, *A&A*, 252, 203
- Sandage, A. 1970, *ApJ*, 162, 841
- Sanders, W. L. 1977, *A&AS*, 27, 89
- Schrijver, C. J. 1987, *A&A*, 172, 111
- Seaton, M. J. 1979, *MNRAS*, 187, 73p
- Shetrone, M. D. 1994, *PASP*, 106, 161
- Shetrone, M. D., & Keane, M. J. 2000, *AJ*, 119, 840
- Simon, T., & Drake, S. A. 1989, *ApJ*, 346, 303
- Simon, T., & Landsman, W. 1991, *ApJ*, 380, 200
- Simon, T., Linsky, J. L., & Stencel, R. E. 1982, *ApJ*, 257, 225
- Smith, G. H., & Churchill, C. W. 1998, *MNRAS*, 297, 388
- Smith, G. H., & Dupree, A. K. 1988, *AJ*, 95, 1547
- Smith, G. H., & Dupree, A. K. 1998, *AJ*, 116, 931
- Smith, G. H., & Janes, K. A. 1988 in *A Decade of UV Astronomy with IUE*, ed. E. J. Rolfe (ESA SP-281, Vol. 2), 193
- Smith, G. H., Dupree, A. K., & Churchill, C. W. 1992, *AJ*, 104, 2005

- Smith, G. H., Dupree, A. K., & Strader, J. 2004, *PASP*, 116, 819
- Soderblom, D. R. 1985, *AJ*, 90, 2103
- Soderblom, D. R., Duncan, D. K., & Johnson, D. R. H. 1991, *ApJ*, 375, 722
- Steiman-Cameron, T. Y., Johnson, H. R., & Honeycutt, R. F. 1985, *ApJ*, 291, L51
- Stencel, R., E., & Mullan, D. J. 1980, *ApJ*, 240, 718
- Stencel, R., E., Mullan, D. J., Linsky, J. L., Basri, G. S., & Worden, S. P. 1980, *ApJS*, 44, 383
- Stone, R. P. S. 1983, *PASP*, 95, 27
- Strassmeier, K. G., Handler, G., Paunzen, E., & Rauth, M. 1994, *A&A*, 281, 855
- Taylor, B. J. 2007, *AJ*, 133, 370
- Wedemeyer-Böhm, S., Steiner, O., Bruls, J., & Rammacher, W. 2007 in *The Physics of Chromospheric Plasmas*, ASP Conf. Ser. 368, eds. P. Heinzel, I. Dorotovič, & R. J. Rutten, 93 (astro-ph/0612627)
- Wilson, O. C., & Bappu, M. K. V. 1957, *ApJ*, 125, 661

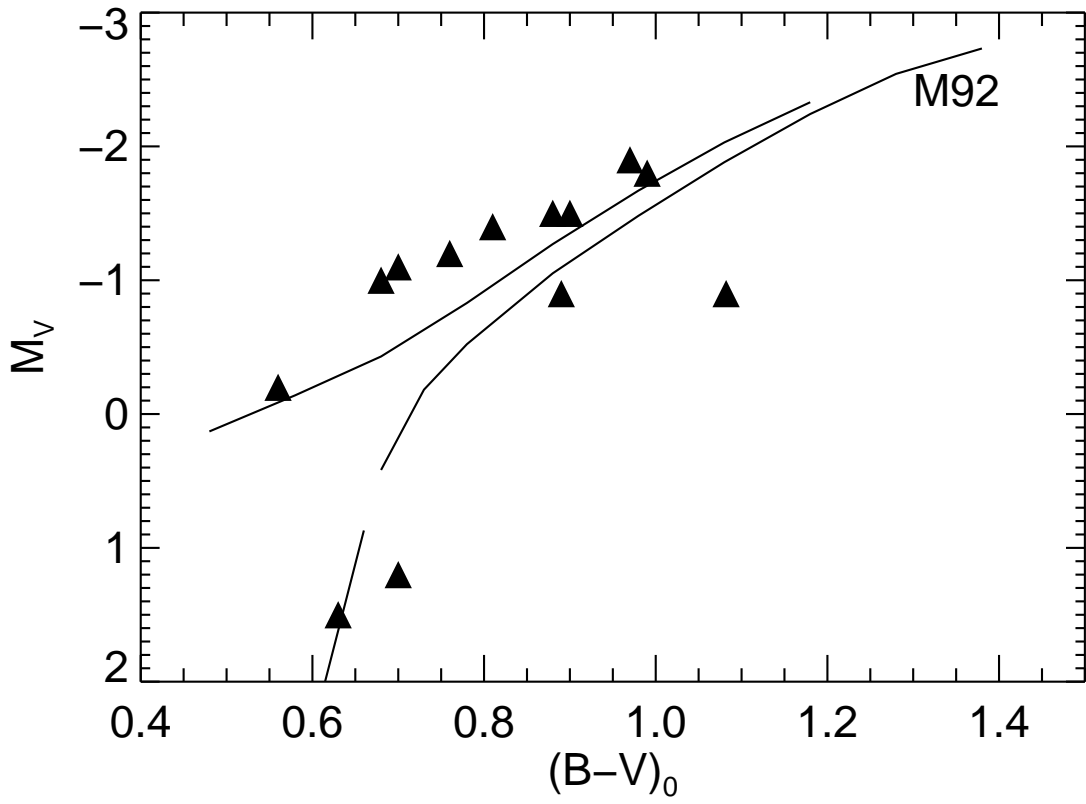


Fig. 1.— Color-magnitude diagram showing the location of the stars discussed in this paper. Solid lines mark the location of the red giant branch, asymptotic giant branch, and subgiant branch in the globular cluster M92 according to Sandage (1970).

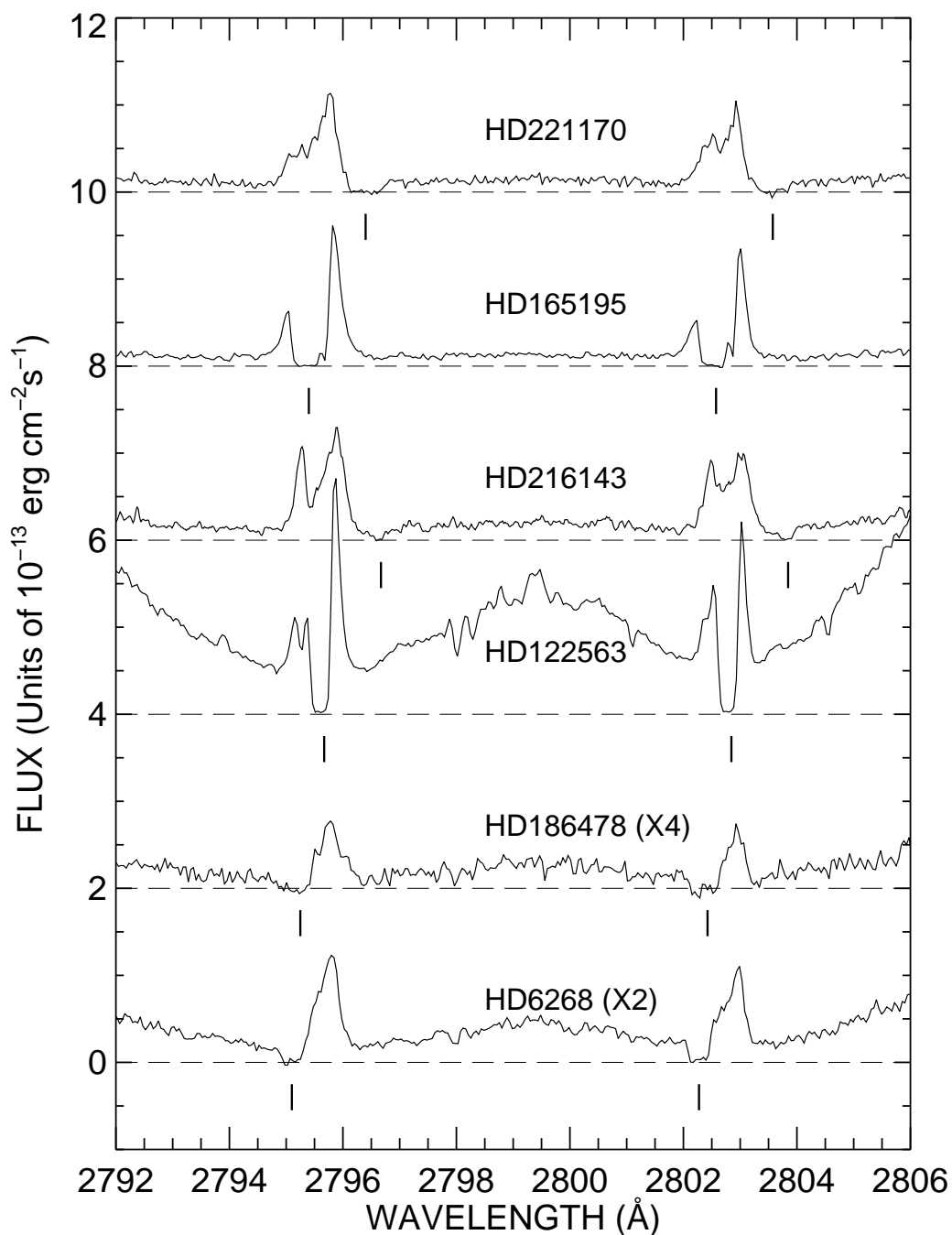


Fig. 2.— Chromospheric emission profiles of the Mg II *h* and *k* lines for stars listed in Table 1. The spectra are arranged from top to bottom in order of decreasing absolute visual magnitude. HD 22170 is the brightest star in the sample at $M_V = -1.9$ and HD 6268 has $M_V = -1.2$. The spectra are aligned on a photospheric wavelength scale. Vertical lines mark the positions of interstellar medium absorption. The flux zero-points are offset by 2×10^{-13} between adjacent spectra, and the spectra of two stars are shown magnified by a factor of 2 or 4. The broken line marks the zero level for each spectrum.

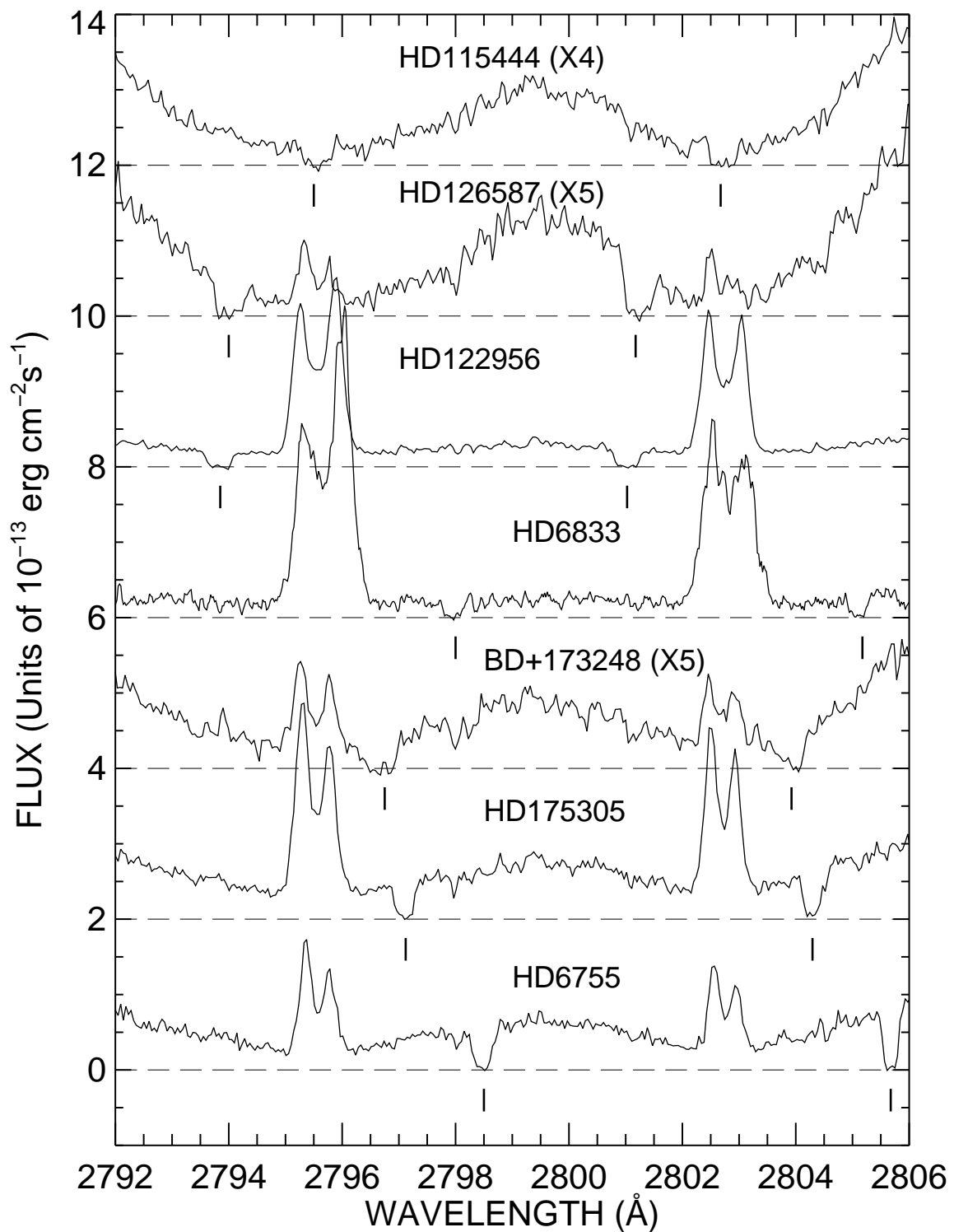


Fig. 3.— Chromospheric emission profiles for the remaining stars from Table 1, with details the same as Fig. 2. Here HD 115444 has $M_V = -1.1$ and HD 175305 and HD 6755 are the two faintest stars in our sample at $M_V = +1.2$ and $M_V = +1.5$ respectively.

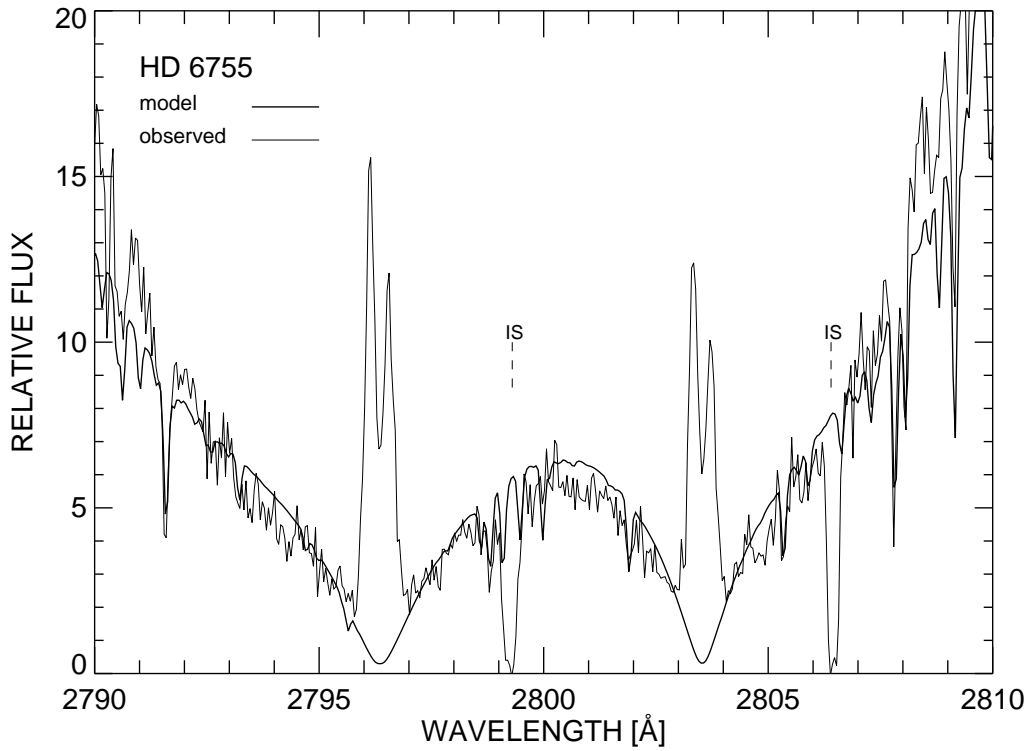


Fig. 4.— Kurucz model synthesis of a photospheric spectrum for HD 6755 overlaid on the observed *HST STIS* spectrum. The agreement between the two spectra is quite good outside of the chromospheric emission profiles. The interstellar Mg II lines are marked as IS.

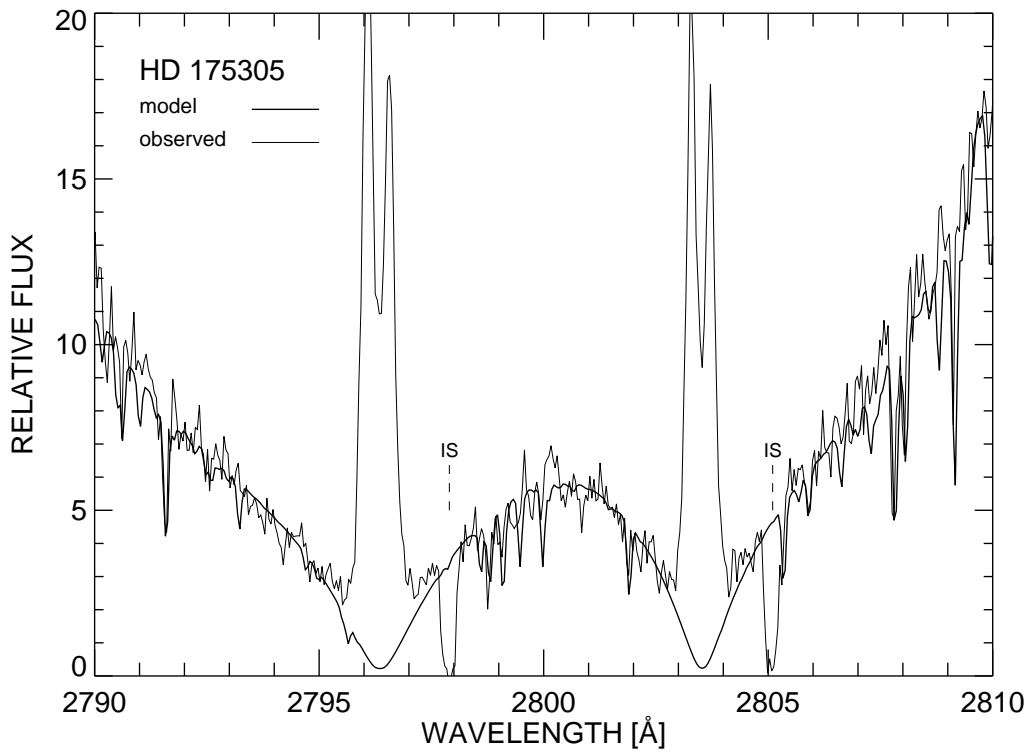


Fig. 5.— Kurucz model synthesis of a photospheric spectrum for HD 175305 overplotted on the *HST STIS* spectrum. IS marks the interstellar Mg II absorption lines.

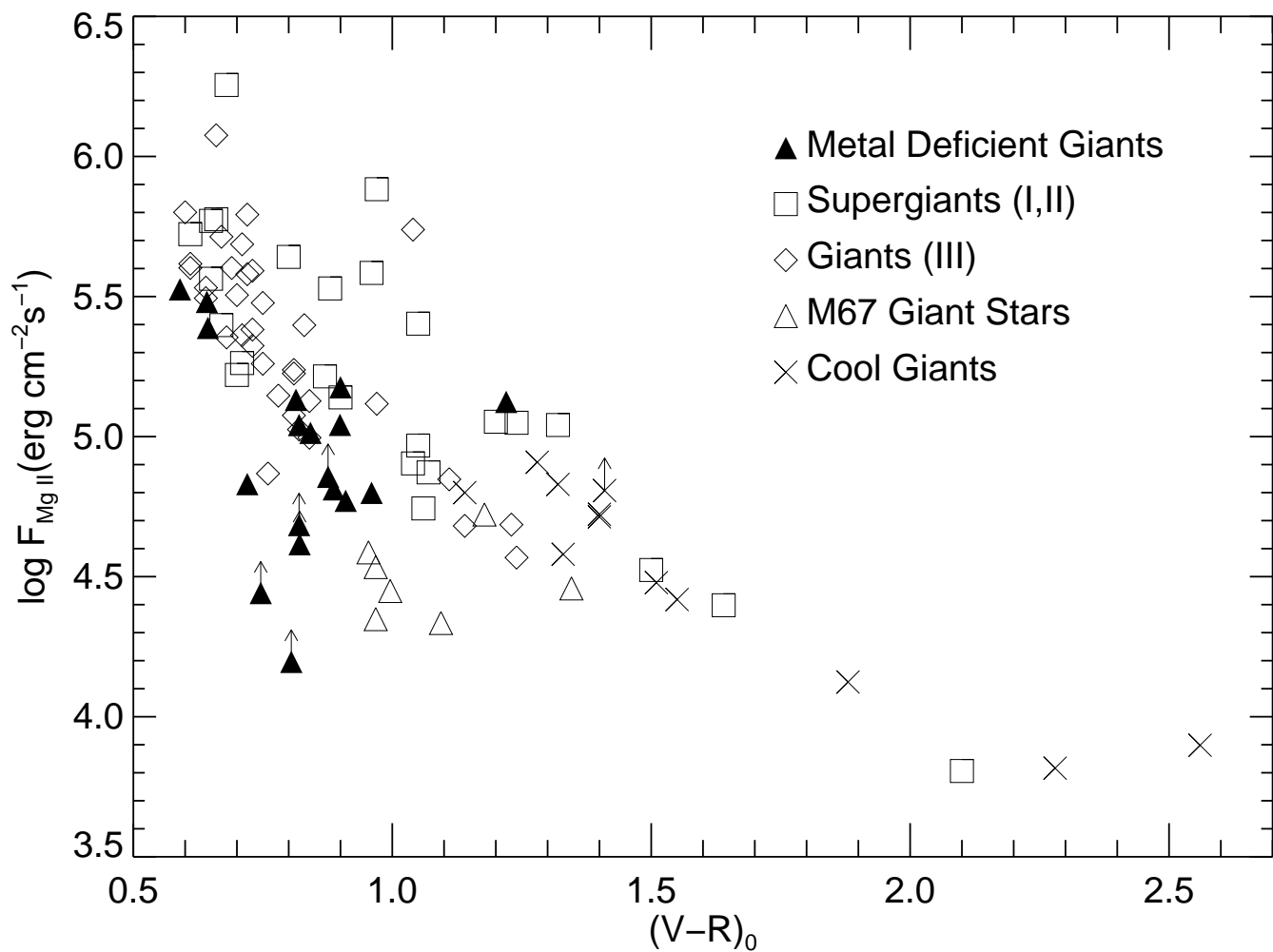


Fig. 6.— Surface Mg II fluxes from the *HST* sample of this paper versus $(V - R)_0$ color. Also shown are data for metal deficient giants reported previously, and Population I field and cluster giants, from Dupree et al. (1990b). The length of the arrows for lower limits to the flux represents a 30% increase in the flux.

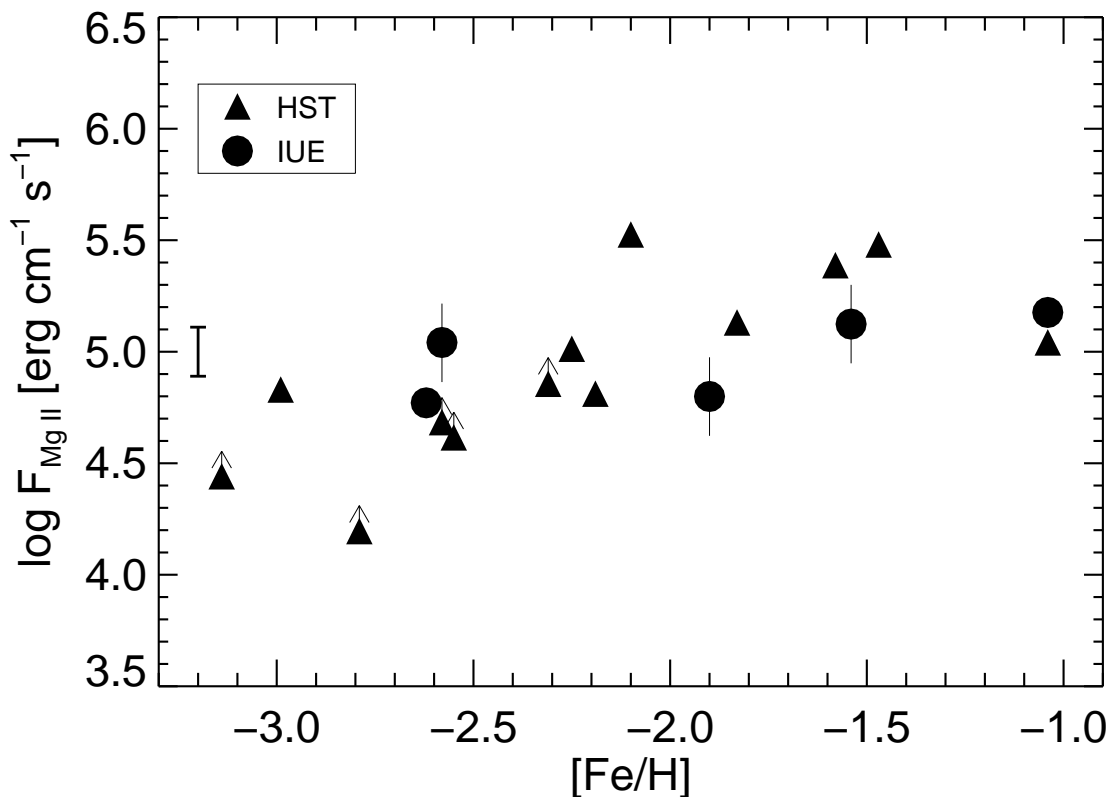


Fig. 7.— Surface Mg II fluxes of the metal deficient giant stars in this sample from *HST* and those studied previously with *IUE* (Dupree et al. 1990b) as a function of metallicity. The error bar shown corresponds to a typical expected error of $\pm 30\%$. Several of the IUE targets had flux errors of $\pm 50\%$ and those are plotted over the symbol. Stars whose profiles may be affected by interstellar Mg II absorption are shown as lower limits, and the length of the arrow represents a 30% increase in the flux.

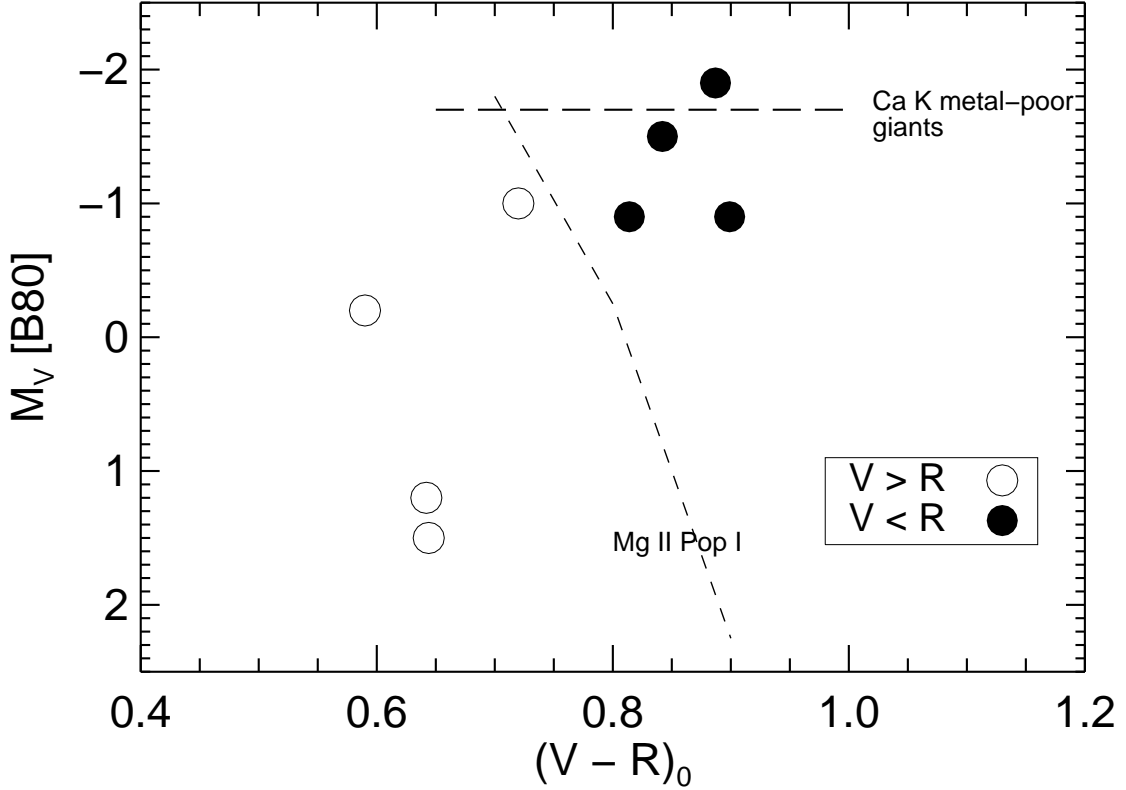


Fig. 8.— Asymmetry of the Mg II k -line emission derived from the *HST* spectra as a function of position in the color-magnitude diagram. The short-dashed line marks the boundary of Mg II asymmetries in Population I stars (Stencel & Mullan 1980; Böhm-Vitense 1981); signatures of outflow occur towards higher $(V-R)$ values. The long-dashed line marks the lower limit of the region where outflow asymmetries ($V/R < 1$) and K_3 -line blueshifts were found in the profile of the Ca II K_2 line of metal-poor red giants by Smith et al. (1992), Dupree & Smith (1995), and Cacciari et al. (2004). Values of M_V and reddening are taken from Bond (1980).

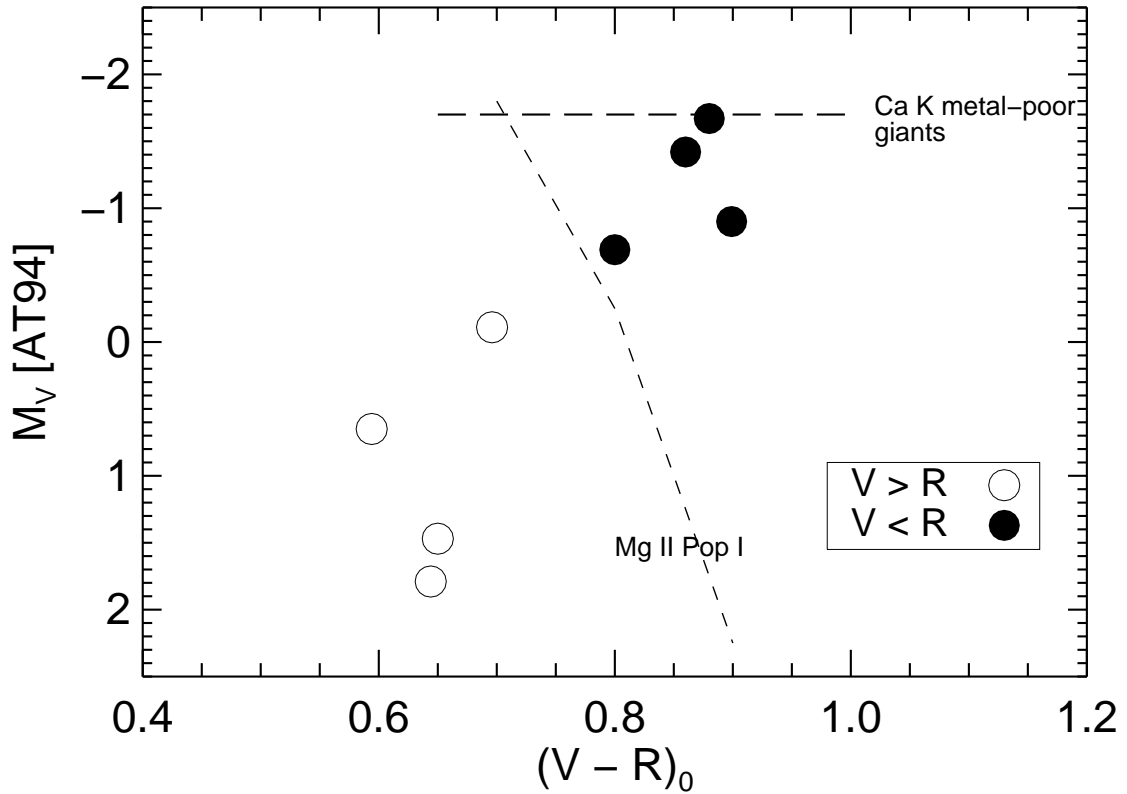


Fig. 9.— Same as Fig. 8, but using the values of M_V and reddening from Anthony-Twarog & Twarog (1994) where $E(V - R) = 1.1E(b - y)$ except for HD 6833 where the Bond (1980) values are assumed. The placement of the stars with respect to the asymmetries found in Population I stars is similar to that using the Bond (1980) values.

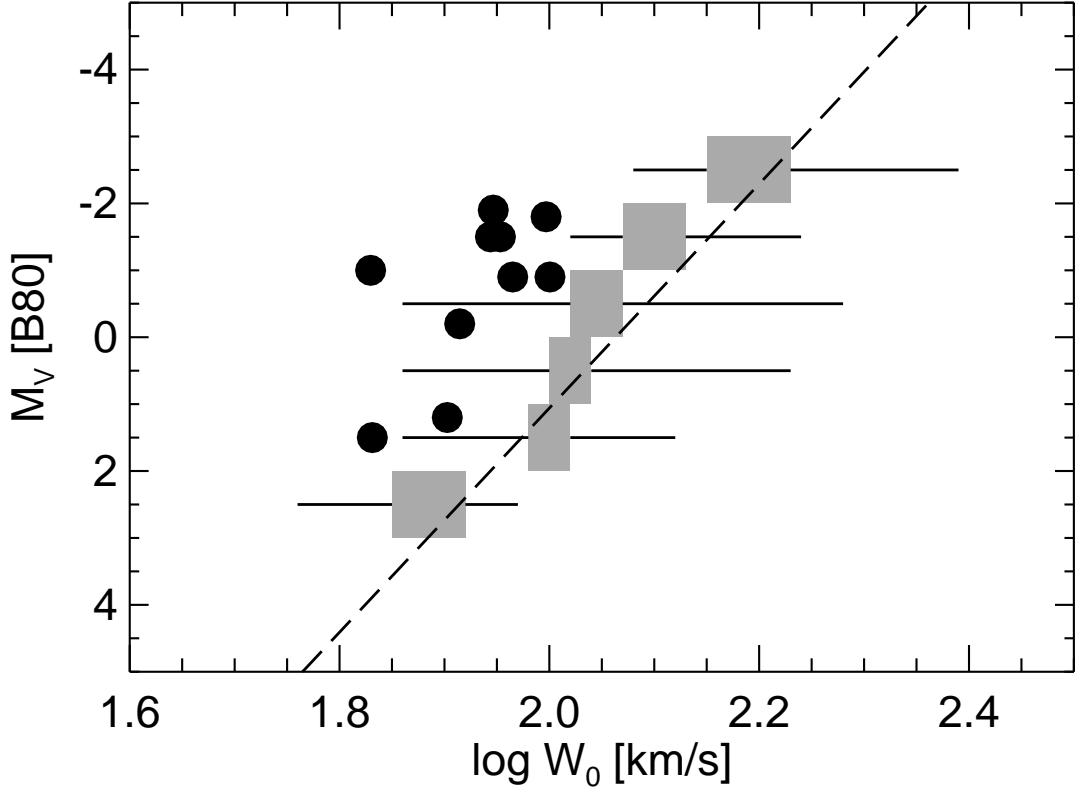


Fig. 10.— Wilson-Bappu width W_0 of the Mg II k line for the metal-poor giants observed by *HST* (filled circles). The shaded region indicates the middle 50% to 67% of the Cassatella et al. sample in $\log W_0$ for the stars in one-magnitude M_V -bins between $M_V = \pm 3$. The horizontal lines mark the total extent of the measurements of line width, again for one-magnitude M_V -bins. The broken line represents the relation obtained by Cassatella et al. (2001) for a large sample of stars observed with *IUE* and *Hipparcos*, including additional brighter and fainter stars not shown in this figure. The metal-deficient giants in our sample, here using the values of M_V from Bond (1980) systematically exhibit smaller values of $\log W_0$.

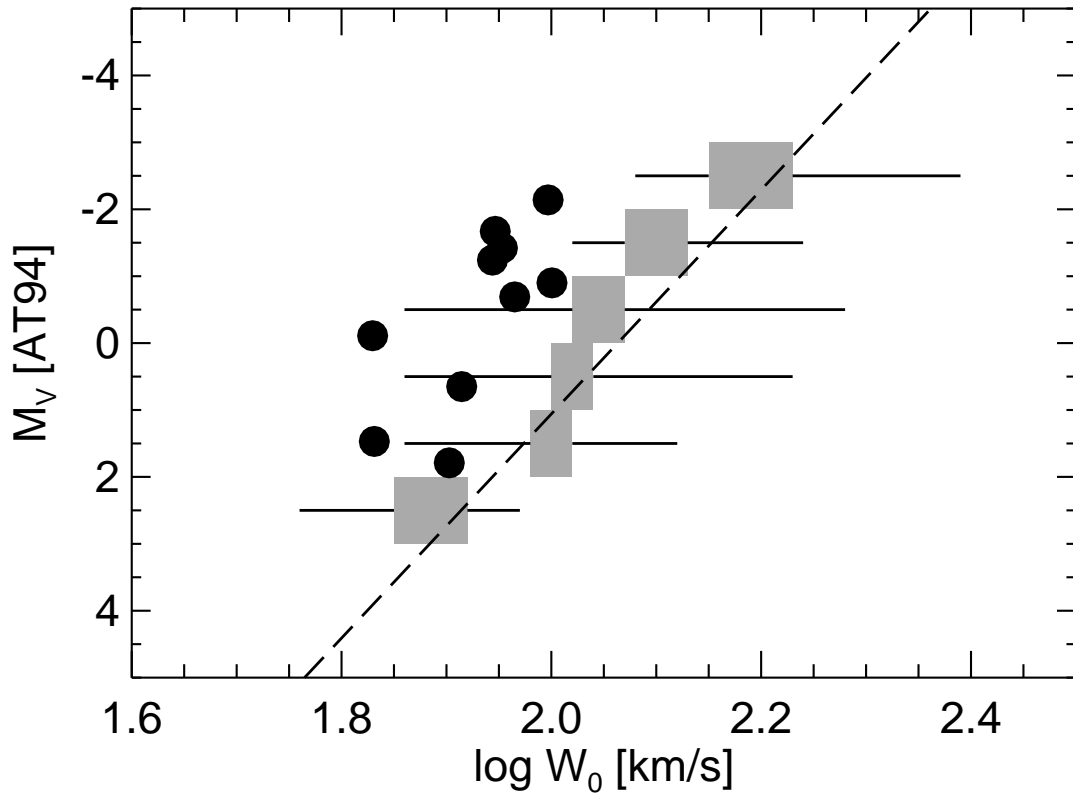


Fig. 11.— Same as Fig. 10 but here using the M_V values obtained by Anthony-Twarog & Twarog (1994) except for HD 6833 where the Bond (1980) values are used. The line widths are systematically smaller than found for Population I field stars.

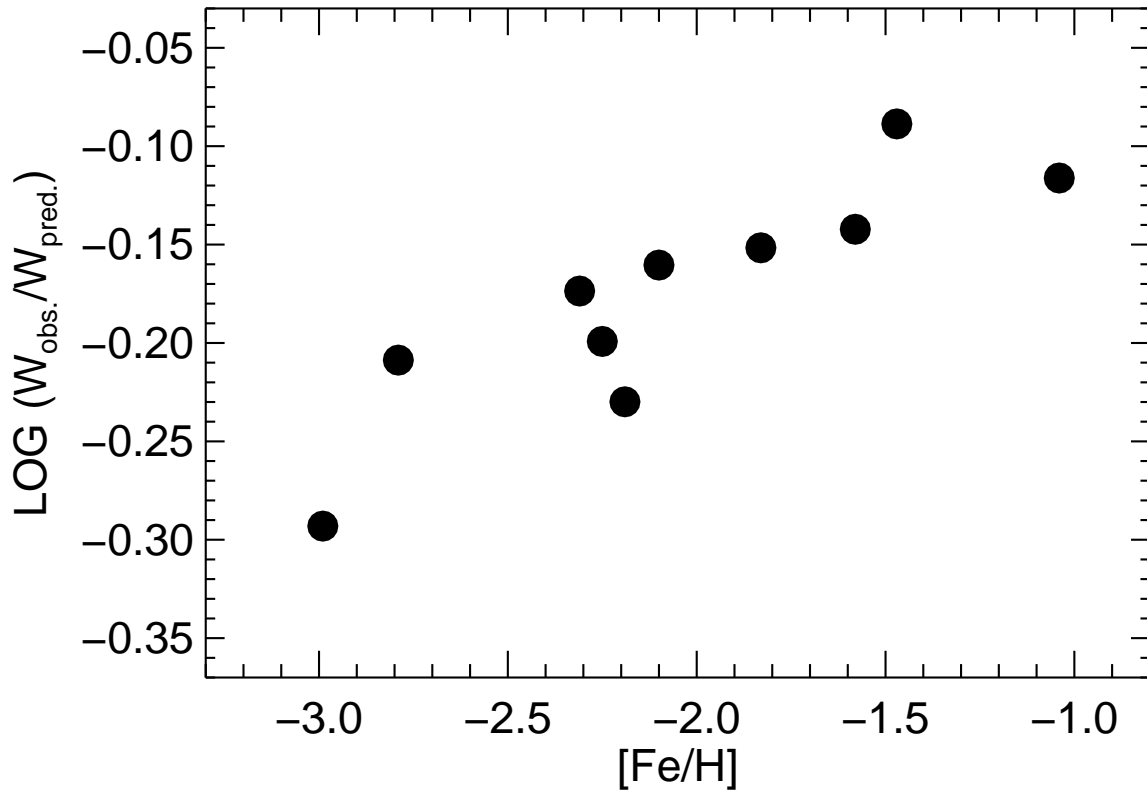


Fig. 12.— Difference between the observed Mg II 2795 Å line width and that predicted by the Cassatella et al. (2001) relation as a function of [Fe/H] for the metal-poor stars in the *HST* sample and selecting the Bond (1980) values (Fig. 10). The trend here suggests that the deviation is metal dependent.

Table 1. Parameters of Target Stars

Star	V^a	$(V - R)_J^b$	$(B - V)^c$	$E(B - V)^a$	M_V^a	V_0^d	$(V - R)_0^e$	Velocity (km s^{-1}) ^f	[Fe/H]	[Fe/H] Ref. ^g	[Fe/H] Ref. ^h
(1)	(2)	(3)	(4)	(5)	(6)	(7)	(8)	(9)	(10)	(11)	(12)
HD 6268 ⁱ	8.11	...	0.79	0.03	-1.2	8.01	0.820 ^j	+38.4	-2.58	1	-2.42
HD 6755	7.73	0.676	0.67	0.04	+1.5	7.60	0.644	-319.2	-1.58	2	-1.68
HD 6833	6.75	0.947	1.14	0.06	-0.9	6.55	0.899	-245.0	-1.04	2	...
HD 115444	8.98	0.746	0.70	0.00	-1.1	8.98	0.746	-28.0	-3.15	3	-2.90
HD 122563	6.21	0.805	0.90	0.00	-1.5	6.21	0.805	-23.2	-2.79	2	-2.72
HD 122956	7.22	0.846	0.93	0.04	-0.9	7.09	0.814	+166.0	-1.83	2	-1.95
HD 126587	9.12	0.76 ^k	0.73	0.05	-1.0	8.96	0.72 ^k	+149.0	-2.99	3	-2.93
BD +17 3248 ⁱ	9.40	0.638	0.62	0.06	-0.2	9.20	0.590	-146.0	-2.11	2	-2.08
HD 165195	7.34	1.076	1.24	0.25	-1.8	6.52	0.876	-0.2	-2.32	3	...
HD 175305	7.20	0.666	0.73	0.03	+1.2	7.10	0.642	-181.0	-1.47	2	-1.48
HD 186478	9.16	0.893	0.90	0.09	-1.4	8.86	0.821	+31.0	-2.58	1	-2.56
HD 216143	7.82	0.874	0.94	0.04	-1.5	7.69	0.842	-116.0 ^a	-2.25	2	...
HD 221170	7.68	0.927	1.02	0.05	-1.9	7.52	0.887	-119.0	-2.19	2	-2.08

^aBond (1980).

^bColor index from Stone (1983) on the Johnson system.

^cSIMBAD database.

^d V magnitude corrected for interstellar extinction assuming $A_V = 3.3E(B - V)$.

^eAssuming $E(V - R)/E(B - V) = 0.8$.

^fSIMBAD database, with the exception of HD 216143, which was acquired from Bond (1980).

^gReferences for [Fe/H] in column 10: (1) McWilliam et al. 1995b; (2) Fulbright 2000; (3) Johnson 2002.

^h[Fe I/H] abundances from Cowan et al. (2005).

ⁱBond notes as AGB star.

^jDupree et al. (1990b).

^kCarney (1980).

Table 2. HST Observations

Star	Dataset	Date Observed	Exposure (s)	Data Type	Mg II K Asymmetry ^a
HD 6268	O5F603010	2001 Jan 31	1870	STIS/E230M	...
	O5F603020	2001 Jan 31	2923	STIS/E230M	
HD 6755	O5F654010	2000 Mar 27	2040	STIS/E230M	$V > R$
HD 6833	Z3GA0106T	1996 Oct 08	577	GHR/G270M	$V < R$
HD 115444	O5F601010	1999 Jul 16	1882	STIS/E230M	...
	O5F601020	1999 Jul 16	11908	STIS/E230M	
	O5F602010	1999 Jul 02	1882	STIS/E230M	
HD 122563	O5EL01010	1999 Jul 29	1767	STIS/E230M	...
	O5EL01020	1999 Jul 29	2887	STIS/E230M	
	O5EL01030	1999 Jul 29	2868	STIS/E230M	
	O5EL01040	1999 Jul 29	2868	STIS/E230M	
HD 122956	O5F605010	1999 Jul 31	1858	STIS/E230M	$V < R$
	O5F605020	1999 Jul 31	2899	STIS/E230M	
HD 126587	O5F606010	2000 Jul 04	1811	STIS/E230M	$V > R$
	O5F606020	2000 Jul 04	11624	STIS/E230M	
HD 165195	O5F608010	1999 Oct 16	1850	STIS/E230M	...
	O5F608020	1999 Oct 16	2899	STIS/E230M	
HD 175305	O5F609010	1999 Aug 22	2195	STIS/E230M	$V > R$
HD 186478	O5F610010	1999 Jun 03	1802	STIS/E230M	...
	O5F610020	1999 Jun 04	11588	STIS/E230M	
	O5F611010	1999 Aug 21	1802	STIS/E230M	
HD 216143	Z3EI0105T	1996 Aug 05	1184	GHR/G270M	$V < R$
	Z3EI0107P	1996 Aug 05	1523	GHR/G270M	
	Z3EI0108T	1996 Aug 05	870	GHR/G270M	
HD 221170	O5F662010	2000 Jul 13	1894	STIS/E230M	$V < R$
BD +17 3248	O5F607010	1999 Oct 15	1802	STIS/E230M	$V > R$
	O5F607020	1999 Oct 15	8691	STIS/E230M	

^a V and R refer to the short-wavelength and long-wavelength sides of the emission core respectively. Asymmetry in the K-line (2795Å) emission could not be assessed in several objects where interstellar absorption affects the line profile.

Table 3. Mg II Fluxes From Metal–Deficient Field Giants

Star	Mg II Observed Flux ^a			ϕ^b	F_*^c	F_*/F_\odot^d	Log W_0^e
	$\lambda 2795$	$\lambda 2802$	Total				
HD 6268	3.11e–14 ^f	2.48e–14 ^f	5.59e–14 ^f	0.482	4.83e+4	0.039	...
HD 6755	9.50e–14	7.53e–14	1.70e–13	0.385	2.44e+5	0.195	1.83
HD 6833	3.03e–13	2.18e–13	5.21e–13	1.062	1.10e+5	0.088	2.00
HD 115444	5.66e–15 ^f	5.60e–15 ^f	1.13e–14 ^f	0.264	2.76e+4	0.022	...
HD 122563	6.91e–14 ^f	3.87e–14 ^f	1.08e–13 ^f	1.082	1.57e+4	0.012	1.94
HD 122956	1.89e–13	1.51e–13	3.40e–13	0.732	1.35e+5	0.108	1.97
HD 126587	1.04e–14	8.54e–15	1.90e–14	0.252	6.77e+4	0.054	1.83
BD +17 3248	1.91e–14	1.51e–14	3.42e–14	0.156	3.36e+5	0.268	1.91
HD 165195	6.35e–14 ^f	4.95e–14 ^f	1.13e–13 ^f	1.044	7.19e+4	0.057	2.00
HD 175305	1.90e–13	1.57e–13	3.48e–13	0.481	3.04e+5	0.242	1.90
HD 186478	9.41e–15 ^f	6.15e–15 ^f	1.56e–14 ^f	0.326	4.13e+4	0.033	...
HD 216143	8.81e–14	7.43e–14	1.62e–13	0.579	1.03e+5	0.082	1.95
HD 221170	6.81e–14	6.05e–14	1.29e–13	0.670	6.48e+4	0.052	1.95

^aUnits of $\text{erg cm}^{-2} \text{s}^{-1}$ observed at Earth. The notation 3.11e–14 denotes 3.11×10^{-14} .

^bStellar angular diameter (in units of 10^{-3} arcsec) from the Barnes, Evans, & Moffett (1978) relation based on $(V - R)$.

^cStellar surface flux in units of $\text{erg cm}^{-2} \text{s}^{-1}$ where $F_* = F_{obs}(d/R_*)^2 = F_{obs} \times 1.702 \times 10^{17}/\phi^2$. F_* has been corrected for reddening (Seaton 1979; Cardelli et al. 1989) where $A_{\lambda 2800} = 6.1E(B - V)$. Reddenings are listed in Table 1.

^dSolar flux in Mg II lines taken as $1.25 \times 10^6 \text{ erg cm}^{-2} \text{s}^{-1}$.

^eThe corrected full width at half power of the Mg II 2795Å line (km s^{-1}).

^fThe stellar radial velocity is $\pm 50 \text{ km s}^{-1}$ or less and so there is potential for absorption by interstellar Mg II. In some case absorption is visible in the line profile. This means the observed Mg II fluxes are lower limits to the stellar fluxes.

Table 4. Mg II Fluxes (IUE) from Metal-Deficient Giants

HD	V^a	$E(B - V)^b$	$(V - R)_0^c$	[Fe/H]	ϕ^c (10^{-3} arcs)	Mg II Obs. ^d ($\text{erg cm}^{-2} \text{s}^{-1}$)	$\log_{10} F_\star^e$ ($\text{erg cm}^{-2} \text{s}^{-1}$)	Refs.
6268	8.11	0.03	0.82	-2.58	0.483	1.1e-13	5.02	1
6833	6.75	0.06	0.90	-1.04	1.062	5.5e-13	5.09	2
84903	8.06	0.13	0.91	-2.60	0.648	1.2e-13	5.00	3
135148	9.49	0.04	0.96	-1.90	0.311	9.9e-14	4.80	4
232078	8.62	0.5:	1.22	-1.54	1.296	8.7e-14	5.17	4

^aBond 1980.

^bBond 1980, except for HD232078 where $E(B - V) = 0.5$: is taken, between values of 0.38 (Beers et al. 2000) and 0.6 (Gonzalez & Wallerstein 1998).

^cStone 1983; value for HD 84903 from Carney 1980.

^dTotal flux in Mg II h and k emission cores observed at Earth with IUE, Dupree et al. 1990b.

^eUnreddened flux from stellar surface using the relations $E_{B-V} = 0.355E_{V-K}$, $A_{\lambda 2800} = 6.1E_{B-V}$ (Seaton 1979).

References. — (1) McWilliam et al. 1995a; (2) Fulbright 2000; (3) Beers et al. 2000; (4) Burris et al. 2000.

Table 5. Mg II Fluxes from Giant and Supergiant Stars

Star	HD	Sp. Type	V^a	$(V - R)^a$	ϕ^b (10^{-3} arcs)	Mg II Obs. ^c ($\text{erg cm}^{-2} \text{s}^{-1}$)	$\log_{10} F_{\star}^d$ ($\text{erg cm}^{-2} \text{s}^{-1}$)	Notes
β Aqr	204867	G0 Ib	2.87	0.61	3.11	3.00e-11	5.72	e
α Aqr	209750	G2 Ib	2.93	0.66	3.44	4.15e-11	5.78	e
β Dra	159181	G2 Ib-IIa	2.78	0.68	3.87	1.58e-10	6.26	f
ξ Pup	63700	G3 Ib	3.35	0.88	4.49	4.0 e-11	5.53	g
9 Peg	206859	G5 Ib	4.31	0.80	2.57	1.70e-11	5.64	f
ϵ Gem	48329	G8 Ib	2.98	0.96	6.00	8.12e-11	5.58	f
56 Peg	218356	K0 Ibp	4.77	0.97	2.67	3.2 e-11	5.88	g
ϵ Peg	206778	K2 Ib	2.39	1.05	8.98	1.2 e-10	5.40	g
λ Vel	78647	K5 Ib	2.21	1.24	12.91	1.1 e-10	5.05	f
ξ Cyg	200905	K5 Ib	3.70	1.20	6.13	2.5 e-11	5.05	g
σ CMa	52877	K7v Ib	3.43	1.32	8.28	4.4 e-11:	5.04	g
α Ori	39801	M2 Iab	0.37	1.64	54.3	4.3 e-10	4.40	h
ϵ Leo	84441	G1 II	2.98	0.65	3.27	3.7 e-11	5.77	g
β Lep	36079	G5 II	2.84	0.65	3.49	2.62e-11	5.56	f
δ Col	44762	G7 II	3.85	0.67	2.31	1.4 e-11	5.40	i
ζ Cyg	202109	G8 II	3.20	0.70	3.36	1.10e-11	5.22	f
ζ Hya	76294	G8 II-III	3.10	0.71	3.61	1.40e-11	5.26	f
θ Lyr	180809	K0 II	4.37	0.87	2.77	7.40e-12	5.21	f
α Hya	81797	K2 II	1.97	1.04	10.7	5.40e-11	4.90	g
γ Aql	186791	K3 II	2.72	1.07	8.0	1.4 e-11	4.87	j
ι Aur	31398	K3 II	2.69	1.06	7.9	1.0 e-11	4.74	j
θ Her	163770	K3 II	3.87	0.90	3.7	5.6 e-12	5.14	j
α TrA	150798	K4 II	1.9	1.05	11.5	3.6 e-11	4.97	j
β Peg	217906	M2 IIb	2.42	1.50	17.2	5.8 e-11:	4.52	g
α Her	156014	M5 II	3.06	2.1:	31.0	3.6 e-11:	3.81:	g
ϵ Hya	74874	G0 III	3.38	0.60	2.40	2.14e-11	5.80	e
o UMa	71369	G5 III	3.36	0.69	3.04	2.2 e-11	5.60	i
μ Vel	93497	G5 III	2.69	0.66	3.84	1.03e-10	6.08	f
η Psc	9270	G7 IIIa	3.62	0.72	2.90	1.9 e-11	5.58	i
β Crv	109379	G7 IIIa	2.64	0.61	3.46	2.91e-11	5.62	f
β Her	148856	G7 IIIa	2.77	0.64	3.51	2.26e-11	5.49	f
ι Cnc	74739	G7.5 IIIa	4.02	0.75	2.61	1.2 e-11	5.48	i
δ Crt	98430	G8 III-IV	3.56	0.83	3.79	2.1 e-11	5.40	i
η Dra	148387	G8 III	2.74	0.61	3.30	2.56e-11	5.60	f
μ Peg	216131	G8 III	3.48	0.68	2.81	1.05e-11	5.35	f
ϵ Vir	113226	G8 IIIb	2.84	0.64	3.40	2.31e-11	5.53	f
η Her	150997	G8 IIIb	3.50	0.67	2.71	2.23e-11	5.71	f
δ Dra	180711	G9 III	3.07	0.70	3.57	2.4 e-11	5.51	i
α Phe	2261	K0 III	2.40	0.81	6.28	4.00e-11	5.24	f
α Cas	3712	K0 IIIa	2.23	0.78	6.44	3.40e-11	5.15	f
ν Oph	163917	K0 IIIa	3.34	0.71	3.23	1.4 e-11	5.36	i
α UMa	95689	K0 IIIa	1.79	0.81	8.31	6.80e-11	5.23	f

Table 5—Continued

Star	HD	Sp. Type	V^a	$(V - R)^a$	ϕ^b (10^{-3} arcs)	Mg II Obs. ^c ($\text{erg cm}^{-2} \text{ s}^{-1}$)	$\log_{10} F_\star^d$ ($\text{erg cm}^{-2} \text{ s}^{-1}$)	Notes
θ Cen	123139	K0 IIIb	2.06	0.76	6.62	1.90e-11	4.87	f
β Gem	62509	K0 IIIb	1.14	0.75	9.86	1.04e-10	5.26	k
β Cet	4128	K1 III	2.02	0.72	6.09	1.35e-10	5.79	f
α Boo	124897	K1+ IIIB	-0.05	0.97	24.56	4.66e-10	5.12	f
β Oph	161096	K2 III	2.77	0.82	5.37	1.80e-11	5.03	f
κ Oph	153210	K2 III	3.20	0.84	4.54	1.20e-11	5.00	f
α Ari	12929	K2 IIIab-b	2.00	0.84	7.89	4.90e-11	5.13	f
α Ser	140573	K2 IIIb	2.64	0.81	5.62	2.21e-11	5.08	f
α Tuc	211416	K3 III	2.85	1.04	7.16	1.65e-10	5.74	f
β UMi	131873	K4 III	2.08	1.11	11.32	5.30e-11	4.85	f
γ Dra	164058	K5 III	2.22	1.14	11.09	3.47e-11	4.68	f
α Tau	29139	K5 III	0.86	1.23	23.69	1.60e-10	4.69	f
β And	6860	M0 III	2.05	1.24	13.90	4.20e-11	4.57	e

^aFrom Johnson et al. 1966.

^bStellar angular diameter obtained from $V, V - R$ (assumed unreddened), and Barnes-Evans-Moffett relationship (1978).

^cTotal flux in Mg II h and k emission cores observed at Earth.

^dFlux from stellar surface.

^eHartmann et al. 1982.

^fSimon et al. 1982.

^gStencel et al. 1980.

^hDupree et al. 1987. The Mg II line in α Ori is variable with a total amplitude of about a factor of 2.

ⁱSimon & Drake 1989.

^jHartmann et al. 1985. Observed flux in the Mg II h -line only. Flux at stellar surface in Mg h has been multiplied by a factor of 2 in order to approximate the contribution of the Mg II k line in the Mg II doublet.

^kBaliunas et al. 1983.

Table 6. Mg II Fluxes from Cool Giant Stars

Star	HD	Sp. Type ^a	V	$(V - R)_0^b$	ϕ^c (10^{-3} arcs)	Mg II Obs. ^d ($\text{erg cm}^{-2} \text{s}^{-1}$)	$\log_{10} F_{\star}^e$ ($\text{erg cm}^{-2} \text{s}^{-1}$)
87 Leo	99998	K4.5 III	4.76	1.14	3.71	5.1 e-12	4.80
74 Gem	61338	M0.0 III	5.05	1.28	2.97	4.20e-12	4.91
HIP 21365	29051	M1.1 III	7.1	1.32	3.01	3.4 e-13	4.83
π Leo	86663	M1.7 III	4.70	1.40	4.88	5.70e-12	4.72
λ Aqr	216386	M2.0 III	3.79	1.40	8.21	1.00e-11	4.71
82 Vir	119149	M2.1 III	5.01	1.33	4.34	4.20e-12	4.58
ν Cap	196777	M2.1 III	5.17	1.41	4.72	>5.00e-12	>4.81
WW Psc	5820	M2.4 III	6.11	1.55	3.16	1.54e-12	4.42
ψ Vir	112142	M2.7 III	4.80	1.51	5.85	3.60e-12	4.48
XZ Psc	224062	M4.6 III	5.61	1.88	6.30	3.12e-12	4.12
HIP 91781	172816	M5.2 III	6.27	2.28	9.03	1.18e-12	3.82
RZ Ari	18191	M5.9 III	5.91	2.56	10.2	4.8 e-12	3.90

^aRidgway et al. 1980.

^bMeasured by Barnes et al. (1978) or derived from $(V - K)_0$ values (Steiman-Cameron et al. 1985) using relation between $(V - K)_0$ and $(V - R)_0$ tabulated by Johnson et al. 1966.

^cOccultation angular diameter (Ridgway et al. 1980).

^dTotal flux in Mg II h and k emission cores observed at Earth (Steiman-Cameron et al. 1985).

^eUnreddened flux from stellar surface using the relations $E_{B-V} = 0.355E_{V-K}$, $A_{\lambda 2800} = 6.1E_{B-V}$ (Seaton 1979).

Table 7. Mg II Fluxes from Cluster Giant Stars

Star	Other Designation	Sp. Type	V^a	$(V - R)_0^b$	ϕ^c (10^{-3} arcs)	Mg II Obs. ^d ($\text{erg cm}^{-2} \text{s}^{-1}$)	$\log_{10} F_\star^e$ ($\text{erg cm}^{-2} \text{s}^{-1}$)
Hyades (C 0424+157)							
ϵ Tau	HD 28305	G9.5 III	3.54	0.73	3.10	1.19e-11	5.32
δ Tau	HD 27697	K0 III	3.76	0.73	2.80	1.11e-11	5.38
θ' Tau	HD 28307	K0 IIIb	3.83	0.71	2.58	1.90e-11	5.69
γ Tau	HD 27371	K0- IIIab	3.65	0.73	2.95	2.00e-11	5.59
M 67 (NGC 2682) ^f							
T-856	BD +12 1917	K2 III:	9.84	0.95	0.269	1.3 e-14	4.59
T-829	BD +12 1913	K2 III	9.53	0.97	0.317	1.6 e-14	4.53
T-626	BD +12 1924	K2 III	9.37	1.09	0.411	1.7 e-14	4.33
F-170	BD +12 1926	K3 III	9.69	0.97	0.294	9.0 e-15	4.35
F-108	TYC 814-2331-1	K4 III	9.72	1.00	0.302	1.2 e-14	4.45
IV-202	BD +12 1919	K5 III	8.86	1.18	0.588	8.5 e-14	4.72
S-1553	BD +11 1934	M0 III	8.74	1.35	0.797	8.5 e-14	4.46

^aHyades: Johnson et al. 1966. M67: Janes & Smith 1984.

^bUnreddened colors on Johnson system. Hyades values from Johnson et al. (1966) where $E(B-V)=0$. M67 values derived from $(V-R)$ observed on Kron-Cousins system and dereddened assuming $E(V-R)/E(B-V) = 0.69$ for K5 giants (Janes & Heasley 1988), $E(B-V) = 0.041$ (Taylor 2007), and the transformation between Kron-Cousins and Johnson $V-R$ colors was made using the equation proposed by Cousins (1976), viz.: $(V-R)_J = 1.40(V-R)_{KC} + 0.028$ for $(V-R)_{KC} < 1$.

^cStellar angular diameter obtained from $V, (V-R)_0$ and Barnes-Evans-Moffett relationship (1978).

^dTotal flux in Mg II h and k emission cores observed at Earth. Hyades: Baliunas et al. 1983. M67: Smith & Janes 1988.

^eUnreddened flux from stellar surface. Stellar surface flux of M67 stars corrected for reddening by assuming $A_{\lambda 2800} = 6.1E(B-V)$ from Seaton (1979), where $E(B-V) = 0.041$ (Taylor 2007). Hyades: $E(B-V) = 0$.

^fStars identified in the following catalogues: T and IV designation: Murray & Clements (1968); F designation: Fagerholm stars identified in Johnson and Sandage (1955); S designation: Sanders (1977).